Journal of Material Sciences & Engineering

Research Article Open Access

Spark Plasma Sintering Techniques Improve the Properties of AlN-TiB_2 Ceramics with Nb_2O_5, Y_2O_3 and ZrO_2 as a Sintering Precursors

José C González[1]*, Miguel A Rodríguez[2], Ignacio A Figueroa[3], María-Elena Villafuerte-Castrejón[3] and Gerardo C Díaz[1]

[1]*Facultad de Ciencias Químicas e Ingeniería, Universidad Autónoma de Baja California, Calzada Tecnológico 14418, Mesa de Otay, Tijuana 22390, Mexico*
[2]*Instituto de Cerámica y Vidrio, CSIC, C/Kelsen 5, 28049 Madrid, Spain*
[3]*Instituto de Investigaciones en Materiales, Universidad Nacional Autónoma de México, Ciudad Universitaria, A.P. 70-360, Ciudad de México 04510, Mexico*

Abstract

AlN-TiB_2 composites ceramics were prepared by Spark Plasma Sintering (SPS). The effects of Nb_2O_5, Y_2O_3 and ZrO_2 additives on mechanical properties and densification were investigated. X-ray diffraction was used to identify the phases in the resulting composites. Good densification results were obtained using the different sintering additives. The mechanical properties such as hardness and fracture toughness were obtained using a Vickers indentation, the maximum values of hardness and fracture toughness were 13.9 ± 0.4 GPa for A4TN (90.48% AlN-4.76% TiB_2-4.76% Nb_2O_5. wt% of composite ceramic) and 5.8 ± 0.9 MPa.$m^{1/2}$ for A23TZ (71.43%AlN-23.81%TiB_2-4.76%ZrO_2 wt% of composite ceramic).

Keywords: Sintering; Densification; Grain growth; Microstructure-property relationship; Spark plasma sintering technique

Introduction

Researchers specializing is materials science continue developing improved and more versatile ceramics for advanced technological applications. The high thermal conductivity and corrosion resistance of aluminium nitride (AlN) in combination with the hardness and electrical conductivity of titanium diboride (TiB_2) allows us to consider the composite AlN-TiB_2 as a promising wear and corrosion resistant ceramics, besides they can be used as the thermocouple protection tube [1,2].

Aluminium Nitride (AlN) ceramics have attracted interest due to their high thermal conductivity and good electrical properties. Their thermal conductivity varies between 80 and 260 $Wm^{-1}K^{-1}$. They exhibit good electrical insulation and have a low dielectric constant (9 at 1 MHz), high thermal conductivity and low thermal expansion coefficient (4.4 x 10^{-6} K^{-1}) [3]. AlN-based materials have a wide field of applications in structural and refractory areas [4].

Titanium diboride (TiB_2) is a material of growing interest among various ultra-high temperature ceramics (UHTC) due to its characteristic high melting point (~3225°C), low density (4.5 g/cm^3), high hardness (25 GPa), high thermal conductivity (96 W/m/K), and electrical conductivity (22 x 10^6 $\Omega^{-1}.cm^{-1}$). Low thermal expansion coefficient (7.4 x 10^{-6} K^{-1}) and high wear resistance [5]. These excellent properties makes it attractive for many high-temperature structural applications [6]. The densification of monolithic TiB_2 requires extremely high sintering temperatures of up to ~2100°C and long holding times due to the predominance of covalent bonding and the low self-diffusion coefficient. Such extreme processing conditions result in exaggerated grain growth of the as-sintered materials, leading to degradation of mechanical properties [7,8].

One way to sinter these materials is through an advanced sintering method such as Spark Plasma Sintering (SPS). During the SPS process, by virtue of special heat effects such as joule heat, electromagnetic field and electrical discharge, highly densified ceramics are obtained at relatively low temperature, in a very short sintering time and with uniform heating for sintered bodies. Functional materials, ceramics, cermets, intermetallic compounds, and so on [9] have been processed by this method.

In this study, for the first time, composites of AlN-TiB_2 were sintered by SPS to evaluate the applicability of SPS techniques in sintering the AlN-TiB_2 composites. The effect of the Nb_2O_5, Y_2O_3 and ZrO_2 content, used as sintering additives, on mechanical properties and densification of composites were also studied in detail.

Materials and Methods

Raw materials

Commercially available AlN powder (grade A100 WR, available from Advanced Refractory Technologies, Buffalo, N. Y., USA), TiB_2 powder (98.64wt%, Storchem, Inc., Burlington, ON, Canada), were used as raw materials. Nb_2O_5 powder (99.5wt%, Strem Chemicals, Newburyport, MA, USA), ZrO_2 powder (99wt%, Strem Chemicals, USA) and Y_2O_3 powder (99.99wt%, Strem Chemicals, USA) were used as sintering additives. The sample compositions studied in this work are shown in Table 1.

Experimental procedure

Powders were homogenized by stirring in a plastic bottle for 4 hours with acetone as dispersant and then were ball milled in a plastic bottle for 25 min with absolute isopropanol as dispersant. After mixing and drying, each of the resulted powders was put into a graphite die of 20 mm in diameter and then sintered in a SPS equipment (Dr. SINTER SPS-1050-CE). During SPS process, both heating and cooling rate were controlled at 150°C/min for all samples. A pressure of 60 MPa from the beginning to the end of the sintering cycle was applied. After 10 min of holding time, samples of 20 mm in diameter and thickness in the 6.9-

***Corresponding author:** José C. González, Facultad de Ciencias Químicas e Ingeniería, Universidad Autónoma de Baja California, Calzada Tecnológico 14418, Mesa de Otay, Tijuana 22390, Mexico, Tel: +52-664-979-7500; E-mail: constantino.gonzalez@uabc.edu.mx

Received October 16, 2019; **Accepted** November 11, 2019; **Published** November 15, 2019

Citation: González JC, Rodríguez MA, Figueroa IA, Villafuerte-Castrejón ME, Díaz GC (2019) Spark Plasma Sintering Techniques Improve the Properties of AlN-TiB_2 Ceramics with Nb_2O_5, Y_2O_3 and ZrO_2 as a Sintering Precursors. J Material Sci Eng 8: 545.

Samples	Starting powders (wt. %)					Preparation Conditions		
	AlN	TiB_2	Nb_2O_5	Y_2O_3	ZrO_2	Sintering Temperature (°C)	Holding Time (min)	Pressure (MPa)
A4TN	90.48	4.76	4.76	-	-	1950	10	60
A14TN	80.95	14.29	4.76	-	-	1950	10	60
A23TN	71.43	23.81	4.76	-	-	1950	10	60
A4TY	90.48	4.76	-	4.76	-	1850	10	60
A14TY	80.95	14.29	-	4.76	-	1850	10	60
A23TY	71.43	23.81	-	4.76	-	1850	10	60
A4TZ	90.48	4.76	-	-	4.76	1950	10	60
A14TZ	80.95	14.29	-	-	4.76	1950	10	60
A23TZ	71.43	23.81	-	-	4.76	1950	10	60

Table 1: Materials compositions and sintering parameters.

Composites	Theoretical density (g/cm³)	Measured density (g/cm³)	Relative density (%)
90.48% AlN – 4.76% TiB_2 – 4.76% Nb_2O_5 (A4TN)	3.45	3.35	97
80.95% AlN – 14.29% TiB_2 – 4.76% Nb_2O_5 (A14TN)	3.59	3.38	94
71.43% AlN – 23.81% TiB_2 – 4.76% Nb_2O_5 (A23TN)	3.50	3.32	95
90.48% AlN – 4.76% TiB_2 – 4.76% Y_2O_3 (A4TY)	3.50	3.36	96
80.95% AlN – 14.29% TiB_2 – 4.76% Y_2O_3 (A14TY)	3.43	3.32	97
71.43% AlN – 23.81% TiB_2 – 4.76% Y_2O_3 (A23TY)	3.62	3.32	92
90.48% AlN – 4.76% TiB_2 – 4.76% ZrO_2 (A4TZ)	3.39	3.38	100
80.95% AlN – 14.29% TiB_2 – 4.76% ZrO_2 (A14TZ)	3.41	3.38	99
71.43% AlN – 23.81% TiB_2 – 4.76% ZrO_2 (A23TZ)	3.58	3.37	94

Table 2: Densities values of the produced composites.

8.9 mm. range were obtained. The sintering temperature was selected after previous sintering cycles, evaluating the density and shrinkage behaviour, using the SPS internal dilatometer.

Characterization and methods

Once the SPS process was completed, the densities of samples were measured in water according to Archimedes´ principle. The relative density was calculated based on the densities of AlN (3.26 g/cm³), TiB_2 (4.52 g/cm³), NbB_2 (6.97 g/cm³), NbN (8.24 g/cm³), Al_2O_3 (3.95 g/cm³), BN (2.10 g/cm³), $Al_{0.9}B_2$ (2.96 g/cm³), TiN (5.40 g/cm³), $Y_3Al_5O_{12}$ (4.56 g/cm³), $YAlO_3$ (5.35 g/cm³) and ZrN (7.09 g/cm³), identified phases by X-ray diffraction, according to the rule of mixtures. Hardness (H_V) of samples were measured at room temperature by the Vickers indentation method; 10 indentations were made on each sample under a load of 1.96 N and a dwell time of 15 s. The Indentation fracture toughness (K_{IC}) of the samples was based on the length of the cracks originating from the edges of the indentation marks using the equations given by Evans and Charles [10] after being carefully polished by standard diamond polishing techniques down to 1 μm finish. 5 indentations were carried out for each sample under a load of 196 N and a dwell time of 15 s.

The crystalline phases were characterized by X-ray diffraction (XRD, Bruker 08 Advance) with Cu Kα radiation. The polished surfaces of the samples were observed by scanning electron microscope (JEOL JSM-7600F, Akishima, Japan) equipped with energy-dispersive spectroscopy (EDS) with a ultra-thin window (UTW) detector to examine the microstructure.

Results and Discussion

According to the literature, the surface of TiB_2 when oxidized forms rutile (TiO_2) and boron oxide (B_2O_3), according to the following reaction [11]:

$$2TiB_{2(s)} + 5O_{2(g)} \rightarrow 2TiO_{2(s)} + 2B_2O_{3(s)} \quad (1)$$

While the surface of AlN is oxidized, alumina (Al_2O_3) and nitrogen (N_2) are formed, according to the following reaction (2):

$$4AlN_{(s)} + 3O_{2(g)} \rightarrow 2Al_2O_{3(s)} + 2N_{2(g)} \quad (2)$$

Table 2 and Figure 1 show the relative density of the obtained composites. It can be observed that as the amount of TiB_2 increases, the relative density decreases, these results confirm again the difficulty to sinter TiB_2. For the samples with Nb_2O_5, the densities obtained were 97% for the sample A4TN, 94% for A14TN and 95% for A_{23}TN. The samples with Y_2O_3 were sintered at 1850°C, obtaining densities of 96% for A4TY, 97% for A14TY and 92% for A23TY by the formation of a liquid phase. ZrO_2 was found to be the best sintering additive for the AlN-TiB_2, obtaining densities of 100% for A4TZ, 99% for A14TZ and 94% for A23TZ.

As shown in Figure 1, the best densification results were obtained with a small amount of TiB_2, as the content of TiB_2 is increased the percentage of densification decreased drastically.

Crystalline Phases

Figure 2 shows the XRD pattern for samples A23TN, A14TN and A4TN sintered by spark plasma sintering at 1950°C for 10 min at an applied pressure of 60 MPa in argon atmosphere. The XRD analysis shows that AlN and TiB_2 are the main phases of all composites. Niobium diboride (NbB_2), niobium nitride (NbN, only in A4TN), alumina (Al_2O_3), hexagonal boron nitride (hBN), aluminum diboride (AlB_2) and titanium nitride (TiN) were identified. The possible reactions for the production of NbB_2, NbN, Al_2O_3 and TiN in the system could be represented as follows:

$$Nb_2O_{5(s)} + 1.2AlN_{(s)} \rightarrow 1.6NbO_{2(s)} + 0.6Al_2O_{3(s)} + 0.4NbN_{(s)} + 0.4N_{2(g)} \quad (3)$$

$$NbO_{2(s)} + TiB_{2(s)} \rightarrow NbB_{2(s)} + TiO_{2(s)} \quad (4)$$

$$3TiO_{2(s)} + 4AlN_{(s)} \rightarrow 3TiN_{(s)} + 2Al_2O_{3(s)} + \tfrac{1}{2}N_{2(g)} \quad (5)$$

Sairam, et al. [12], obtained NbB_2 by spark plasma sintering at

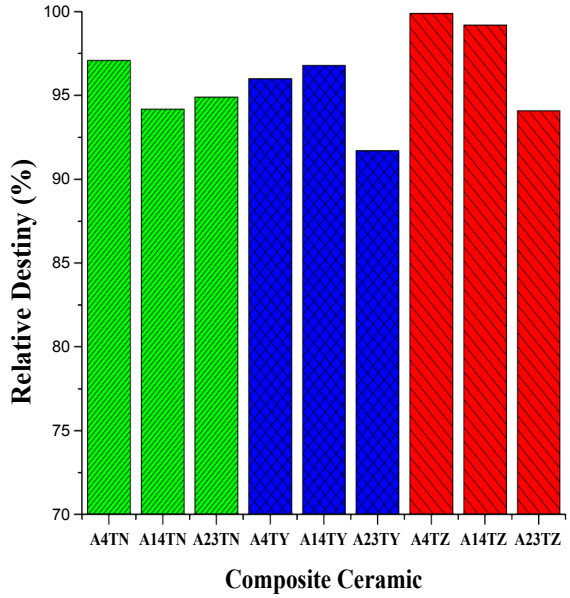

Figure 1: Relative density of the composite ceramics.

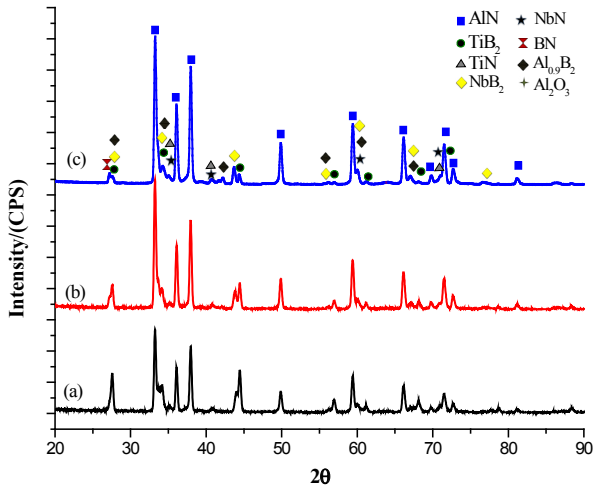

Figure 2: XRD patterns of sintered AlN-TiB_2 samples with Nb_2O_5: (a) A23TN; (b) A14TN; (c) A4TN.

1900°C, obtaining 97.7%ρ_{th}. With the synthesis of NbB_2 (4) with hexagonal crystal structure in the sintering process, the high densities in the samples with Nb_2O_5 could be explained.

The presence of hBN and TiN, is attributed to the reaction of N_2 (reactions 3 and 5) with TiB_2:

$$TiB_{2(s)} + \tfrac{3}{2}N_2 \rightarrow TiN_{(s)} + 2BN_{(s)} \quad (6)$$

The presence of AlB_2 and TiN, was attributed to the following reaction:

$$TiB_{2(s)} + AlN_{(s)} \rightarrow AlB_{2(s)} + TiN_{(s)} \quad (7)$$

In reaction (7) the aluminum diboride was assigned the formula "AlB_2", it was found that the density of such phase was 2.955 g/cm^3, which corresponds to $Al_{0.9}B_2$, not to AlB_2, which has a theoretical density of 3.17 g/cm^3 [13].

Figure 3 shows the XRD pattern for samples A23TY, A14TY and A4TY sintered by spark plasma sintering at 1850°C for 10 min at an applied pressure of 60 MPa in an argon atmosphere. The XRD analysis showed that AlN and TiB_2 are the main phases. However, $Al_{0.9}B_2$ was identified as a secondary phase in all samples, i.e. $Y_3Al_5O_{12}$ (YAG) in A4TY and A14TY, $AlYO_3$ (YAP) in A14TY and A23TY. In addition, TiN and BN were found in samples A14TY and A23TY. No peaks of TiN and BN were found in samples A4TY.

The existence of TiN and BN in the samples A14TY and A23TY can be related to the presence of TiO_2 in the surface layer of the TiB_2 particles, which reacted with the AlN in the sintering process according to the reaction (5), the N_2 from nitride reacted with TiB_2 according to reaction (6). Only a limited amount of TiN and BN was formed in the sintering process under argon, since only a limited amount of TiO_2 was available [14].

Figure 4 shows the XRD pattern for samples A23TZ, A14TZ and A4TZ sintered by spark plasma sintering at 1950°C for 10 min at an applied pressure of 60 Mpa under an argon atmosphere. The XRD analysis showed that AlN and TiB_2 were the main phases for all composites. As secondary phases, zirconium nitride (ZrN), alumina (Al_2O_3), boron nitride (BN) and titanium nitride (TiN) were identified. Aluminum diboride ($Al_{0.9}B_2$) was identified in samples A23TY and A14TY.

The real process to explain the presence of ZrN is complex but it should be modelized with the following reactions [15]:

$$4AlN_{(s)} + 3ZrO_{2(g)} \rightarrow 3ZrN_{(s)} + 2Al_2O_{3(s)} + \tfrac{1}{2}N_{2(g)} \quad (8)$$

$$2AlN_{(s)} + 2ZrO_{2(g)} \rightarrow 2ZrN_{(s)} + Al_2O_{3(s)} + \tfrac{1}{2}O_{2(g)} \quad (9)$$

Microstructural Analysis

Figure 5a-5c shows SEM micrographs of polished surfaces of the A4TN, A14TN and A23TN ceramics, respectively. It was observed in Figure 5 that AlN-TiB_2- Nb_2O_5 ceramics were mainly composed of three dark, gray and white phases. The elemental composition was obtained through EDS analysis at point A and point B in Figure 5a, as shown in Figure 6. The EDS of Figure 6a and 6b revealed that the dark

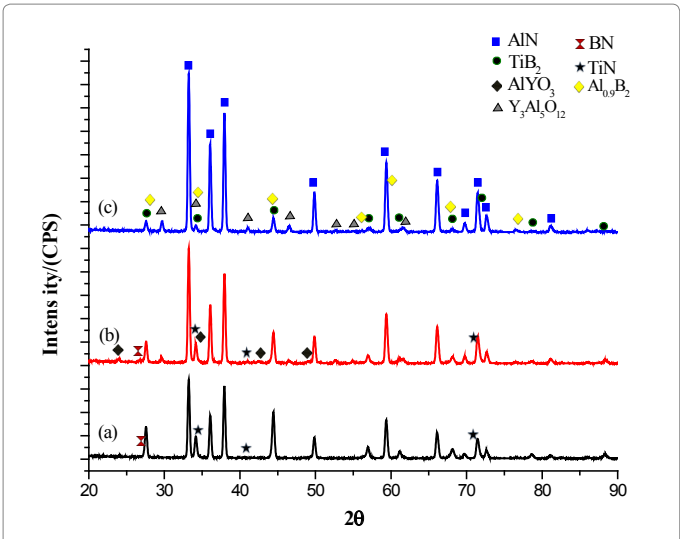

Figure 3: XRD patterns of sintered AlN-TiB_2 samples with Y_2O_3: (a) A23TY; (b) A14TY; (c) A4TY.

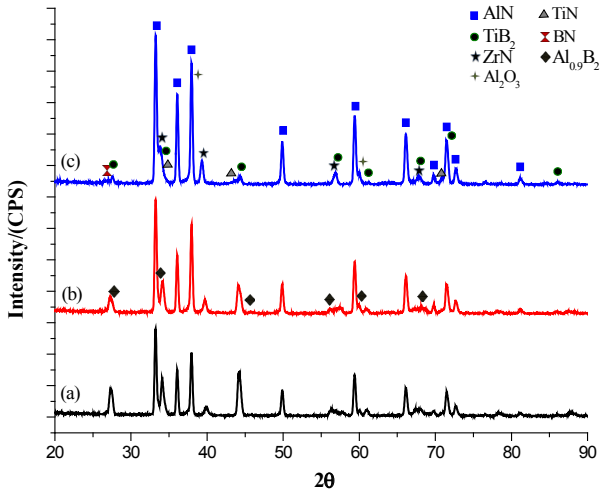

Figure 4: XRD patterns of sintered AlN-TiB_2 samples with ZrO_2: (a) A23TZ; (b) A14TZ; (c) A4TZ.

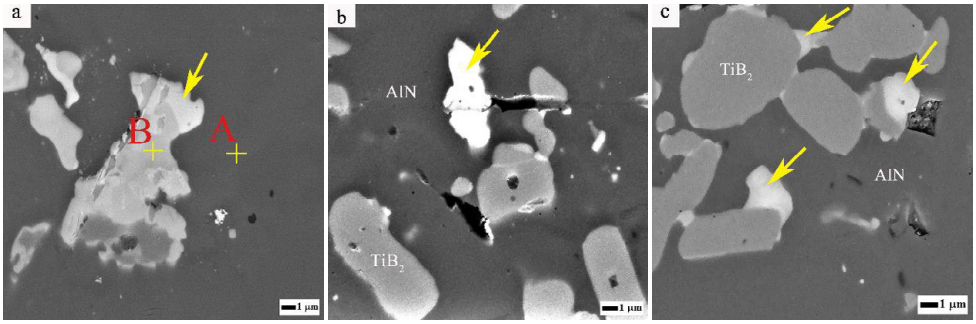

Figure 5: SEM micrographs of ceramic composites (a) A4TN, (b) A14TN and (c) A23TN. The grain pattern was observed on polished surfaces of composite ceramics.

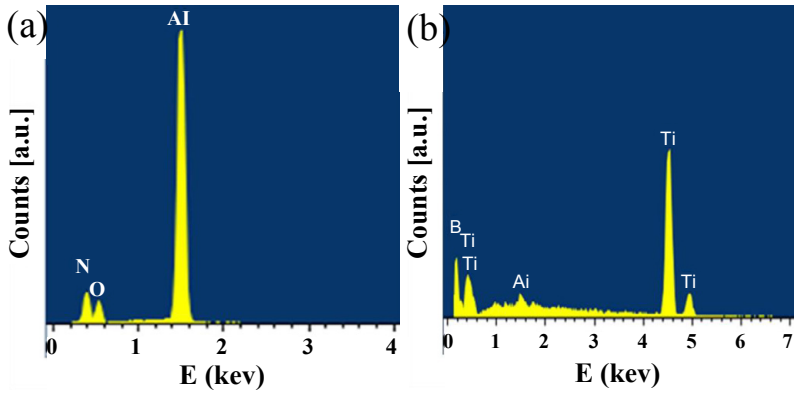

Figure 6: EDS spectrums of AlN-TiB_2 ceramic composites corresponding to (a) Point A and (b) Point B in Figure 5 (a).

phase, point A in Figure 5a, consisted mostly of Al and N elements and the gray phase, point B in Figure 5a, predominantly contained Ti and B elements, indicating that the dark phase was AlN and the gray phase TiB_2.

Some white phases were also observed among the AlN grains and TiB_2 grains in the composites A4TN, A14TN and A23TN (marked with arrows in Figure 5). In order to deeply clarify the phases, EDS analyses were employed (Figure 7). It was concluded with the support of XRD patterns, SEM-EDS that AlN, TiB_2, NbB_2, NbN, were found in A4TN. Al_2O_3, hBN, $Al_{0.9}B_2$ and TiN phases were observed in A4TN, A14TN and A23TN composites.

Figure 8a-8c shows SEM micrographs of polished surfaces of the AlN-TiB_2-Y_2O_3 composites with different amounts of TiB_2, A4TY, A14TY and A23TY. The AlN grains were composed with a yttria-based secondary phase. TiB_2 grains were randomly dispersed in the AlN matrix. EDS analyses showed that dispersed gray particles are TiB_2.

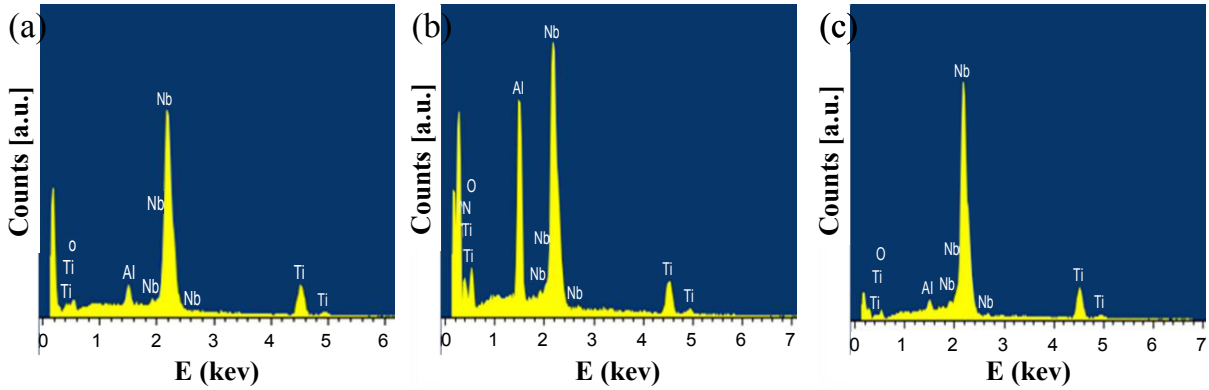

Figure 7: EDS spectrums of (a) A4TN, (b) A14TN and (c) A23TN composites corresponding to arrows in Figure 5 (a)-(c) respectively.

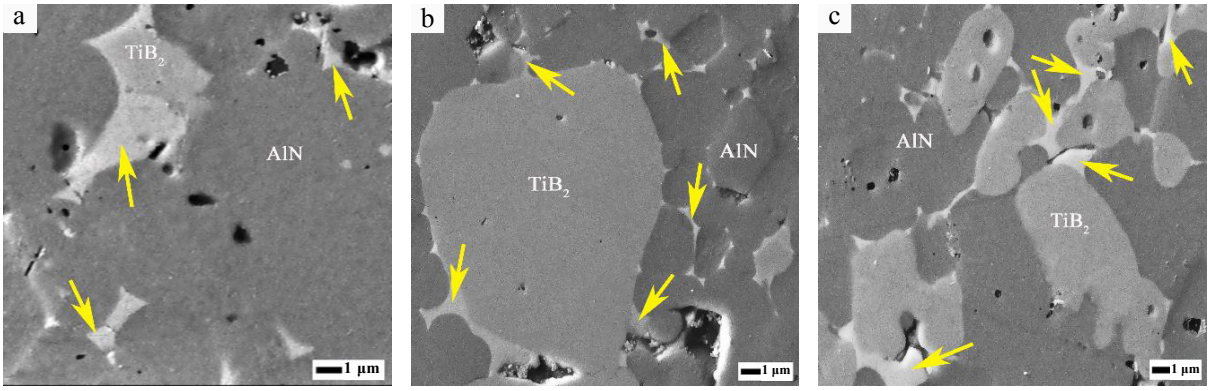

Figure 8: SEM micrographs of ceramic composites (a) A4TY, (b) A14TY and (c) A23TY. The grain pattern was observed on polished surfaces of composite ceramics.

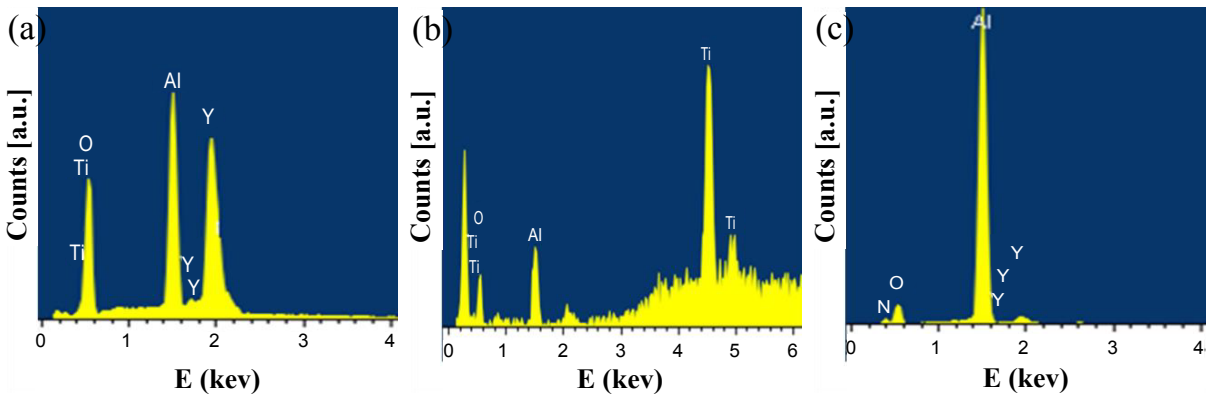

Figure 9: EDS spectrums of (a) A4TY, (b) A14TY and (c) A23TY composites corresponding to arrows in Figure 8 (a)-(c) respectively.

The grain pattern was observed on polished surfaces of composite ceramics.

According to the EDS analyses (Figure 9) the white particles, were attributed to yttria-based secondary phase (marked with arrows in Figure 8a-8c). As shown in Figure 8, the presence of Y_2O_3 as a sintering additive forms with Al_2O_3, from the Surface of AlN, an eutectic composition that helps sintering and normally precipitates as YAG, diffuses between the particles, which helps to achieve highly dense materials. The interesting point is to observe that the results of the densification are not very high in comparison with other oxides used as additives, this may be due to the fact that grain growth is controlled by diffusion at the grain edge.

Figure 10a-10d displays the SEM micrographs of polished surfaces of the composites A4TZ, A14TZ and A23TZ, respectively. From this figure, it is observed that AlN-TiB_2 composite was mainly composed of three phases. The chemical composition of the gray and dark zones were identified by EDS. Several white phases were observed among AlN and TiB_2 grains (see arrows in Figure 10a-10c), these analyzed by EDS (Figure 11). The results revealed that the microstructure consists predominantly of zirconium. Therefore it was concluded with supports

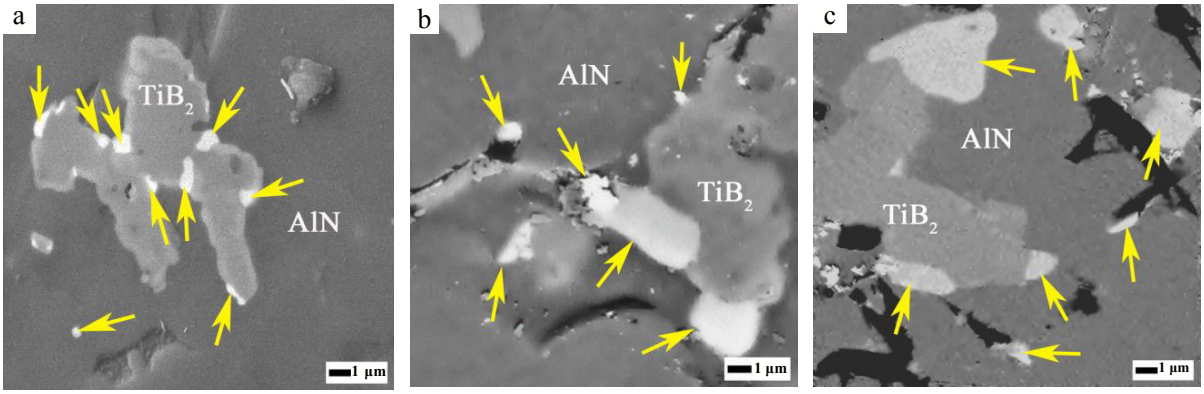

Figure 10: SEM micrographs of ceramic composites (a) A4TZ, (b) A14TZ and (c) A23TZ. The grain pattern was observed on polished surfaces of composite ceramics.

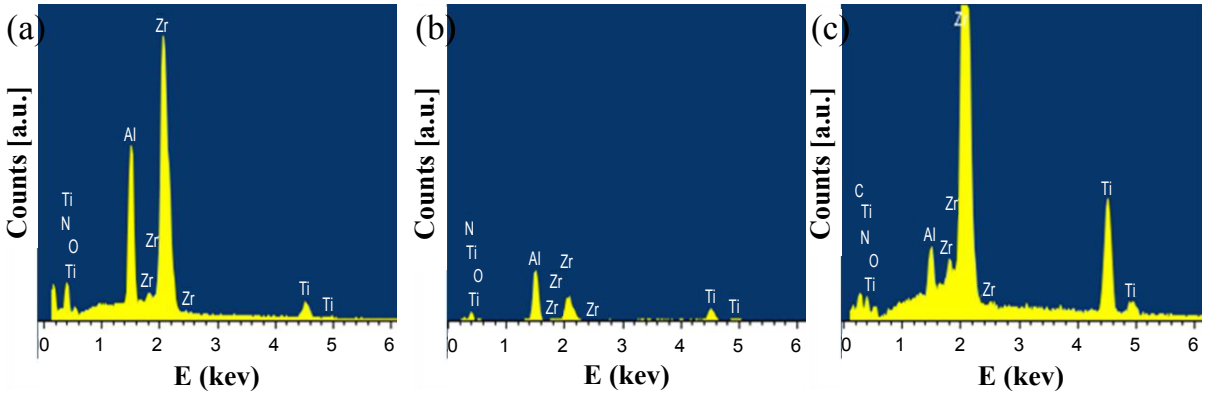

Figure 11: EDS spectrums of (a) A4TZ, (b) A14TZ and (c) A23TZ composites corresponding to arrows in Figure 10 (a)-(c) respectively.

of XRD patterns, and SEM-EDS that AlN, TiB_2, ZrN, Al_2O_3, BN and TiN phases are the main contributors of the three composites, besides the phase $Al_{0.9}B_2$ was found only in the A14TZ and A23TZ composites.

Mechanical Properties

Table 3 shows the mechanical properties of the sintered composites. The hardness results for all composites were found to be above to that of the monolithic AlN, but well below to the magnitude of the TiB_2 value. The fracture toughness of the composites was improved when compared to the value of the monolithic AlN. The composites A23TN, A14TZ and A23TZ showed higher fracture toughness, surpassing the fracture toughness value of the monolithic TiB_2. The fracture toughness of the composites, exceeded the values reported in our previous paper, using the same amount of Nb_2O_5, Y_2O_3 and ZrO_2 [16,17].

Figure 12 shows the hardness and fracture toughness measurements for the sintered samples. It is noteworthy that all the samples have a higher hardness that of the monolithic AlN due to the contribution of TiB_2 phase. A significant increase of the hardness was observed in the samples that contain Nb_2O_5 (A4TN, A14TN and A23TN), this could be a consequence of a remarkable presence of nitrides, identified by the XRD spectrum. The presence of a mixture of NbB_2 [10] and NbN phases [18] increased the hardness. It can also be observed that as the amount of TiB_2 increased to 14.29 wt.%, the hardness in the samples sintered with Nb_2O_5 and ZrO_2 decreased, being attributed to the high

Composites	Hv (GPa)	K_{IC} (MPa.m$^{1/2}$)
AlN	10.6[a]	3.2[a]
TiB_2	25[a]	5.2[b]
A4TN	13.9 ± 0.4	4.3 ± 0.4
A14TN	12.8 ± 0.5	4.4 ± 0.6
A23TN	13.1 ± 0.4	5.4 ± 0.9
A4TY	10.7 ± 0.2	4.5 ± 0.6
A14TY	11.5 ± 0.4	4.7 ± 0.6
A23TY	11.9 ± 0.4	4.8 ± 0.9
A4TZ	12.7 ± 0.3	3.8 ± 0.4
A14TZ	12.4 ± 0.3	5.5 ± 0.8
A23TZ	12.9 ± 0.3	5.8 ± 0.9

[a,b] Values taken from the reference [3,17], respectively.

Table 3: Results of the mechanical properties for the composites.

covalent character of TiB_2 and its difficulty to be sintered properly, increasing the porosity and the grains growth, reducing the density and hardness. In the sample sintered with Y_2O_3, it was observed that as the amount of TiB_2 increased, the hardness also increased. This result was associated to the formation of a secondary liquid phase (YAG and YAP), which diffuses between the grains of AlN and TiB_2, acting as an elastic interface.

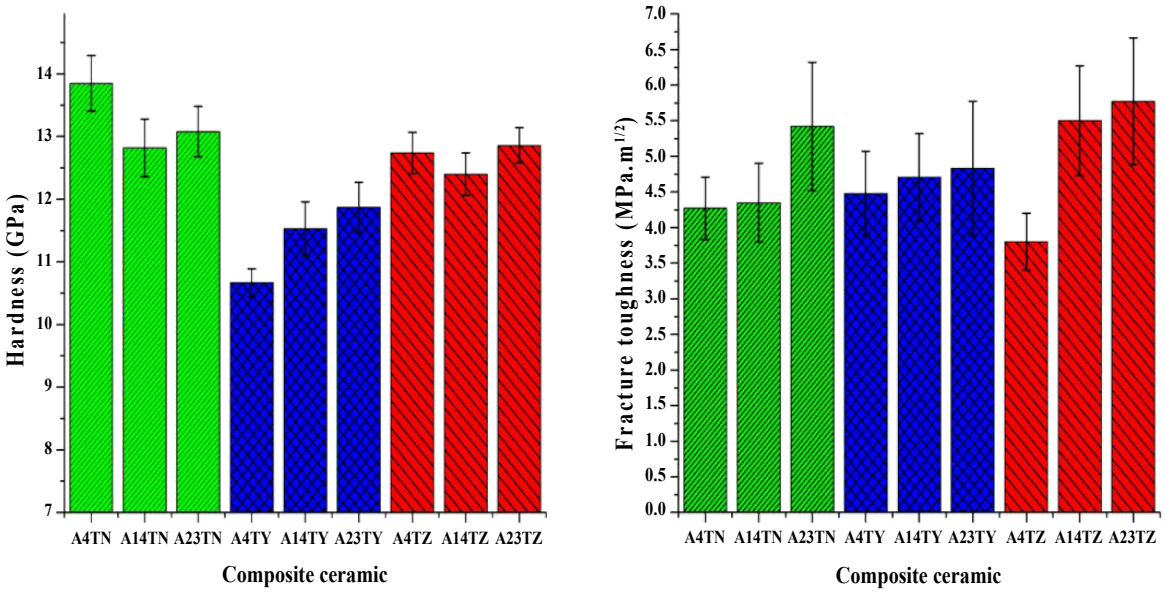

Figure 12: Mechanical properties of ceramic composites: (a) hardness and (b) fracture toughness.

Conclusions

The sintering of AlN-TiB_2 with Nb_2O_5, Y_2O_3 and ZrO_2 as sintering additives, was achieved by SPS, obtaining excellent densification results, increasing the values of hardness and fracture toughness with respect to the monolithic AlN. The ceramic composites that showed the best densification results were A4TZ and A14TZ, with values up to 100% of theoretical density.

With respect to mechanical properties, higher values of hardness and fracture toughness were obtained when compared to those of the monolithic AlN. The composites that showed the highest hardness were A4TN and A23TN, with values of 13.9 ± 0.4 GPa and 13.1 ± 0.4 GPa, respectively. Regarding fracture toughness, it was observed that it increased when the amount of TiB_2 increased. Therefore, the composites with a content of 23.81% of TiB_2 showed the best results.

Acknowledgements

The authors would like to thank Angel de Pablos Perez of the Instituto de Cerámica y Vidrio, CSIC-Spain for assistance in SPS. Adriana Tejeda, Omar Novelo of the Instituto de Investigaciones en Materiales of the Universidad Nacional Autónoma de México by XRD and SEM and Héctor Damián Orozco of the Universidad Michoacana de San Nicolás de Hidalgo for measurements of fracture toughness.

References

1. Chao W, Xiangxin X, Xiaozhou C, Lu Z, Jian Z, et al. (2013) A New method of fabricating AlN-TiB2 composite ceramics. Mater Manuf Process 28: 953-956.
2. Podehernyaeva IA, Panasyuk AD, Lavrenko VA, Andrievskii RA, Teplenko MA, et al. (2001) Structure and properties of composite electrospark, laser, and magnetron deposited AlN-TiB2 coatings. Pow Metall Metal Ceram 40: 501-508.
3. Zhang XY, Tan SH, Jiang DL (2005) AlN-TiB2 composites fabricated by spark plasma sintering. Ceram Int 31: 267-270.
4. Auger MA, Sánchez O, Albella JM (2006) Recubrimientos protectores de TiN y AlN: comportamiento frente a temperatura. Bol Soc Esp Ceram V 45: 75-79.
5. Subramaniam C, Murthy TSRCh, Suri AK (2007) Synthesis and consolidation of titanium diboride. Int J Refract Met Hard Mater 25: 345-350.
6. Sánchez JM, Azcona I, Castro F (2000) Propiedades mecánicas de cermets basados en diboruro de titanio. Bol Soc Esp Cerám V 39: 251-254.
7. Mukhopadhyay A, Raju GB, Basu B, Suri AK (2009) Correlation between phase evolution, mechanical properties and instrumented indentation response of TiB2-based ceramics. J Eur Ceram Soc 29: 505-516.
8. Basu B, Raju GB, Suri AK (2006) Processing and properties of monolithic TiB2-based materials. Int Mater Rev 51: 352-374.
9. Song SX, Wang Z, Shi GP (2013) Heating mechanism of spark plasma sintering. Ceram Int 39: 1393-1396.
10. Moradkhani A, Baharvandi H, Tajdari M, Latifi H, Martikainen J (2013) Determination of fracture toughness using the area of micro-crack tracks left in brittle by vickers indentation test. J Adv Ceram 2: 87-102.
11. Tampieri A, Bellosi A (1993) Oxidation of monolithic TiB2 and of Al2O3-TiB2 composite. J Mater Sci 28: 649-653.
12. Sairam K, Sonber JK, Murthy TSRCh, Subramanian C, Fotedar RK, et al. (2014) Reaction spark plasma sintering of niobium diboride. Int J of Refract Met Hard Mater 43: 259-262.
13. Whittaker ML, Cutler RA (2013) Effect of synthesis atmosphere, wetting, and compaction on the purity of AlB2. J Solid State Chem 201: 93-100.
14. Xu GF, Carmel Y, Olorunyolemi T, Lloyd IK, Wilson Jr OC (2003) Microwave sintering and properties of AlN/TiB2 composites. J Mater Res 18: 66-76.
15. Toy C, Savrun E (1998) Novel composites in the aluminum nitride-zirconia and hafnia systems. J Eur Ceram Soc 18: 23-29.
16. González JC, Rodríguez MA, Figueroa IA, Villafuerte-Castrejón ME, Díaz GC (2017) Development of AlN and TiB2 composites with Nb2O5, Y2O3 and ZrO2 as sintering aids. Materials 10: 324.
17. Zhang ZH, Shen XB, Wang FC, Lee SK, Wang L (2010) Densification behavior and mechanical properties of the spark plasma sintered monolithic TiB2. Ceramics Mater Sci Eng A 527: 5947-5951.
18. Oliveira RM, Oliveira AC, Carreri FC, Gomes GF, Ueda M, et al. (2013) Detailed surface analyses and improved mechanical and tribological properties of niobium treated by high temperature nitrogen plasma based ion implantation. Appl Surf Sci 283: 382-388.